IN-34

TECHNICAL MEMORANDUM

X-235

AN EXPERIMENTAL INVESTIGATION AND CORRELATION OF THE HEAT

REDUCTION TO NONPOROUS SURFACES BEHIND A POROUS LEADING

EDGE THROUGH WHICH COOLANT IS EJECTED

By William G. Witte and Bernard Rashis

Langley Research Center
Langley Field, Va.

Declassified April 23, 1962

NATIONAL AERONAUTICS AND SPACE ADMINISTRATION

WASHINGTON   March 1960

NATIONAL AERONAUTICS AND SPACE ADMINISTRATION

TECHNICAL MEMORANDUM X-235

AN EXPERIMENTAL INVESTIGATION AND CORRELATION OF THE HEAT

REDUCTION TO NONPOROUS SURFACES BEHIND A POROUS LEADING

EDGE THROUGH WHICH COOLANT IS EJECTED*

By William G. Witte and Bernard Rashis

SUMMARY

A configuration of a wing segment having constant chord thickness, $0°$ sweep, a porous steel semicircular leading edge, and solid Inconel surfaces was tested in a Mach number 2.0 ethlyene-heated high-temperature air jet. Measurements were made of the wing surface temperatures at chordwise stations for several rates of helium flow through the porous leading edge. The investigation was conducted at stagnation temperatures ranging from $500°$ F to $2,400°$ F, at Reynolds numbers per foot ranging from 0.3×10^7 to 1.2×10^7, and at angles of attack of $0°$, $\pm 5°$, and $\pm 15°$.

The results indicated that the reduction of wing surface temperatures, with respect to their values for no coolant flow, depended on the helium coolant flow rates and the distance behind the area of injection. The results were correlated in terms of the wall cooling parameter and the coolant flow-rate parameter, where the nondimensional flow rate was referenced to the cooled area up to the downstream position.

For the same coolant flow rate, lower surface temperatures are achieved with a porous-wall cooling system. However, since flow-rate requirements decrease with increasing allowable surface temperatures, the higher allowable wall temperatures of the solid wall as compared to the structurally weaker porous wall, sharply reduce the flow-rate requirements of a downstream cooling system. Thus, for certain flight conditions it is possible to compensate for the lower efficiency of the downstream or solid-wall cooling system. For example, a downstream cooling system using solid walls that must be maintained at $1,800°$ F would require less coolant for Mach numbers up to 5.5 than would a porous-wall cooling system for which the walls must be maintained at temperatures less than or equal to $900°$ F.

---

*Title, Unclassified.

INTRODUCTION

A solution to the problem of aerodynamic heating of wing structures at high flight Mach numbers may be found through the incorporation of some type of cooling system. Two cooling systems which have been investigated previously are transpiration cooling (ref. 1) and upstream ejection cooling (ref. 2). In upstream ejection cooling, the coolant is ejected through a tube at the stagnation point and forms a shroud or film over the surface to be cooled. In transpiration cooling, the coolant passes through as well as over the cooled surface. The coolant comes into intimate contact with the surface and is then ejected into the boundary layer. The temperature and velocity profiles of the boundary layer are altered and the heat transfer through the boundary layer is reduced. The present model utilizes a small section of porous material for the leading edge. The purposes of the present investigation were (1) to measure, for different test conditions, the reduction in heating on solid surfaces located behind a porous leading edge and (2) to correlate the results of the various tests in terms of parameters readily determined for any full-scale flight condition.

SYMBOLS

c_p specific heat, Btu/lb-$^\circ$F

d diameter of cylindrical leading edge, in.

F ratio of coolant weight flow rate to free-stream weight flow rate, $\dfrac{w/S}{(\rho V)_l}$

h heat-transfer coefficient, Btu/(sq ft)(sec)($^\circ$F)

M Mach number

N_{St} Stanton number

p pressure, psia

S cooled area, sq ft

s distance downstream from porous leading-edge flat-plate juncture, in.

T	temperature, $^{\circ}$F unless otherwise noted
V	velocity, ft/sec
w	total mass-flow rate, lb/sec
x	distance downstream from stagnation point on porous leading edge, measured along surface, in.
α	angle of attack, deg
γ	ratio of specific heats
η	boundary-layer recovery factor
ρ	density, lb/cu ft

Subscripts:

aw	adiabatic wall
c	coolant
w	equilibrium conditions pertaining to skin of model
l	conditions outside boundary layer
o	zero coolant flow rate
pw	porous wall
sw	solid wall
t	total conditions
t_2	total conditions behind normal shock
wall	conditions pertaining to skin of model
∞	free-stream conditions

TEST FACILITY AND PROCEDURE

The present investigation was conducted in a Mach number 2.0 ethylene-heated high-temperature air jet. This facility is capable of producing stagnation temperatures ranging from 900° F to 3,500° F by burning mixtures

of ethylene and air. The air is initially heated to 500° F and is then passed into a combustion chamber where it is mixed with the ethylene gas. Complete details of this facility are given in reference 3.

The model was mounted on a catapult sting as shown in figure 1. Before injection of the model into the stream, steady-state conditions were achieved in the tunnel flow and in the flow of helium through the model. After injection of the model into the stream, the helium flow was adjusted, when necessary, to the preinjection flow rate. The tests were of sufficient duration to achieve equilibrium values of the model surface temperatures.

Model and Instrumentation

The model used in these tests is shown in figure 2. The leading edge was made by bending a flat piece of 1/16-inch-thick porous stainless steel into the semicircular shape. Three thermocouples were attached to the inside of this porous strip for temperature measurements. These thermocouples failed mechanically during the initial stages of testing and no useful data were obtained from them.

The wing surfaces of the model were constructed of 0.050-inch-thick flat-plate Inconel. These were instrumented with pressure tubes and thermocouples of No. 30 (American wire gage) chromelalumel wire as indicated in figure 2.

The wing surfaces were supported internally by two 0.050-inch-thick Inconel bulkheads to prevent buckling at high temperatures. Both bulkheads were placed an inch from the thermocouple center line, in order to minimize temperature errors due to conduction of heat to these supports.

A backing plate of 0.050-inch-thick Inconel separated the leading edge internally from the rearward part of the wing section. The ends of the two 1/4-inch helium supply lines were welded to this plate. Thus, no coolant came into contact with the internal wing surfaces.

A perforated half-cylinder strip was placed between the porous leading edge and the backing plate to facilitate the distribution of the helium coolant along the porous leading edge. A pressure tube and a thermocouple were installed near this perforated strip in order to measure the temperature and pressure of the helium inside the model.

A flowmeter, a thermocouple, and a pressure tap were installed in the coolant supply line between the model and the helium supply tanks in order to measure the total mass flow of helium going into the model.

Data Reduction

For the tests at 0° angle of attack, the model center line coincided with the center line of the jet. The total mass flow of coolant ejected through the porous leading edge was divided equally with one-half the coolant flowing over one wing surface and one-half flowing over the other wing surface. For angles of attack of 5° and 15°, the porous leading edge was not alined symmetrically with the flow and the calculated amount of the total mass flow which flowed over the compression side was considerably less than that which flowed over the expansion side. No means were available for measuring the percentage distribution of the total coolant mass flow. However, the mass flow of coolant through a porous material is essentially inversely proportional to the pressure on the outside of the porous material. Thus, the percentage distribution of the coolant flow was assumed equal to the ratio of the integrated values of the reciprocals of the surface pressures for the two sides. Although these ratios actually depend somewhat on the actual value of the pressure inside the model, the variation in the ratios was less than 2 percent for two cases which were computed considering the inside pressure values. If the surface pressures given in figure 3 (fig. 9 of ref. 4) are used, the distribution of the coolant flow was roughly 37 percent and 19.5 percent for the compression sides at angles of attack of 5° and 15°, respectively, and 63 percent and 80.5 percent for the expansion sides.

The faired surface-pressure distributions on the wing surfaces as a function of distance from the porous-leading-edge flat-plate juncture and angle of attack are shown in figure 4. In the tests at angles of attack of 5° and 15°, the surface containing five pressure tubes was the compression side.

The local mass-flow values were calculated from

$$(\rho V)_l = (\rho V)_\infty \frac{p_l}{p_\infty} \frac{M_l}{M_\infty} \sqrt{\frac{T_\infty}{T_l}}$$

The ratio $(\rho V)_l / (\rho V)_\infty$ as a function of distance from the porous-leading-edge flat-plate juncture and angle of attack are shown in figure 5.

The heat-transfer coefficients for zero coolant flow as a function of distance from the porous-leading-edge flat-plate juncture and angle of attack are shown in figure 6. The stagnation temperature for these tests was approximately $1,000^\circ$ F, for which $\gamma = 1.3$ (ref. 5).

The variation of the heat-transfer ratio for zero coolant flow as a function of angle of attack is shown in figure 7. Measured values

for two thermocouple stations are indicated by test points. The solid line shows values that were calculated according to the procedure given in reference 6.

The values of T_{aw}, the boundary-layer recovery temperature for zero coolant flow, were computed by using a recovery-factor value of 0.88.

The nondimensional flow rate F was computed from

$$F = \frac{w/S}{(\rho V)_l}$$

where w was the total flow in pounds per second over the cooled surface and S was the area from the porous-leading-edge flat-plate juncture to the downstream thermocouple stations.

The specific heat values for helium and air used in the correlation parameter $\left(F/N_{St,o}\right)\left(c_{p,c}/c_{p,l}\right)$ were obtained from reference 7. The term $c_{p,c}$ was evaluated at the cooled wall temperature, and the term $c_{p,l}$ was evaluated at the local temperature.

RESULTS AND DISCUSSION

Figures 8, 9, and 10 show typical temperature time histories for thermocouple stations along the flat-plate wing surfaces. For the test at 0° angle of attack, the temperatures on both wing surfaces of the model were essentially equal; therefore, the temperature time history for only one surface was plotted. In all tests the temperatures for all stations reached equilibrium values. The calculated adiabatic (or zero flow) values are also shown. It should be noted that the equilibrium temperatures along both surfaces of the model, for all three angles of attack, become successively higher with increasing distance from the leading edge. For the test at 5° angle of attack, the temperatures on the compression side are higher than the temperatures at the same thermocouple stations on the expansion side. For 15° angle of attack, the temperatures on the compression side are markedly higher than the temperatures on the expansion side. In fact, for the test at 15° angle of attack, the temperature at the thermocouple station farthest from the leading edge on the expansion side is lower than the temperature at the first thermocouple station on the compression side. It should be noted that the ratios of weight flow of helium passing over the expansion side to the weight flow of helium passing over the compression side are roughly 5/3 for 5° angle of attack and 4/1 for 15° angle of attack.

Although the total temperatures and weight flows of helium are almost the same for both the compression sides at $\alpha = 5^\circ$ and 15°, the equilibrium temperatures along the flat plate are higher for the 15° case than for the 5° case, due to the higher adiabatic wall temperature for the 15° case. It should be noted that for all the tests of the present investigation, the porous wall temperatures were approximately the same as the initial temperatures of the helium coolant, which was essentially at ambient temperature.

Figure 11 shows typical curves of the wall cooling parameter $\dfrac{T_w - T_c}{T_{aw} - T_c}$ plotted against s/d, the distance behind the porous-leading-edge flat-plate juncture divided by the diameter of the leading edge, for angles of attack of 0°, 5°, and 15°. For the case of 0° angle of attack, the curve rises sharply at first, indicating a rapid decrease in cooling along the wing surface behind the porous leading-edge flat-plate juncture. The curve then becomes more gradual, indicating a more gradual decrease in the cooling. The curves for the compression sides at $\alpha = 5^\circ$ and 15° are similar to the curve for $\alpha = 0^\circ$ but are higher and rise more sharply; this indicates that the cooling is less and decreases more rapidly than for $\alpha = 0^\circ$. The curves for the expansion sides at $\alpha = 5^\circ$ and 15° are lower and less curved than for $\alpha = 0^\circ$; this indicates that the cooling is greater and decreases more gradually than for the $\alpha = 0^\circ$.

Figures 12(a), 12(b), and 12(c) show the wall cooling parameter $\left(T_w - T_c\right)/\left(T_{aw} - T_c\right)$ plotted against the coolant flow-rate parameter $\left(F/N_{St,o}\right)\left(c_{p,c}/c_{p,l}\right)$ for angles of attack of 0°, 5°, and 15°, respectively. The data were separated as to angle of attack for clarity. The faired curves for figures 12(a), (b), and (c) are the same. The use of these parameters enabled correlation of all the test results.

Figure 13 shows the curves for downstream cooling and for transpiration cooling of a completely porous wing surface (ref. 1). The curve for a completely porous wing surface is lower than the curve for downstream cooling; this shows that, for the same flow rate of coolant, lower wall temperatures are achieved on the surface of the completely porous material than on the solid surfaces of a downstream cooling system. However, it should be noted that the maximum allowable temperature that porous stainless steel may reach before deteriorating is approximately 900° F, whereas the maximum allowable temperature for solid material would be much higher. Since for the same heating environment, increasing the allowable surface temperature will sharply decrease the flow-rate requirements, it is possible, for certain flight conditions, to compensate for the lower efficiency of the solid-wall cooling system.

Figure 14 illustrates this compensating effect for the case where the maximum allowable temperature of the porous material is 900° F. The region above the curve represents the conditions for which the higher allowable temperature of the solid wall decreases the flow-rate requirements below the value required to maintain a porous material at 900° F. For a solid steel surface, T_{sw}/T_{pw} is approximately 2.0, thus a downstream system using solid steel walls maintained at 1,800° F would require less coolant for Mach numbers up to 5.5. The procedure for computing the curve of figure 14 is given in the appendix.

CONCLUDING REMARKS

Through use of the wall cooling parameter and the coolant flow-rate parameter, where the nondimensional flow rate is the total flow ejected divided by the cooled area up to the downstream position, the temperature distributions on a solid surface behind a porous leading edge through which helium was ejected were correlated. There were no effects on the correlation due to stagnation-temperature variation or angle-of-attack variation.

For the same coolant flow rate, lower surface temperatures are obtained with a porous-wall cooling system. However, since flow-rate requirements decrease with increasing allowable surface temperatures, the higher allowable wall temperatures of the solid wall, as compared to the structurally weaker porous wall, sharply reduce the flow-rate requirements of a downstream cooling system. Thus, it is possible, for certain flight conditions, to compensate for the lower efficiency of the downstream or solid-wall cooling system. For example, a downstream cooling system using solid steel walls maintained at 1,800° F requires less coolant for Mach numbers up to 5.5 than would a porous-steel-wall cooling system for which the walls must be maintained at temperatures less than or equal to 900° F.

Langley Research Center,
    National Aeronautics and Space Administration,
        Langley Field, Va., October 28, 1959.

APPENDIX

PROCEDURE FOR OBTAINING CURVE IN FIGURE 14

In this section, the details of the procedure for obtaining the curve shown in figure 14 are given. The curve of figure 14 represents the specific case of where the porous-wall temperature is maintained at 900° F. Also, the curve of figure 14 is somewhat restrictive since, in order to simplify the computations, it was assumed that the coolant and local airstream temperatures were equal, and it was also assumed that γ was constant (1.4) for the Mach number range. By definition

$$T_{aw} = T_l\left(1 + \eta \frac{\gamma - 1}{2} M_\infty^2\right)$$

the parameter $\left(T_w - T_c\right)/\left(T_{aw} - T_c\right)$ can be written as

$$\frac{\left(T_w - T_c\right)}{\left\{T_l\left(1 + \eta \frac{\gamma - 1}{2} M_\infty^2\right) - T_c\right\}} = \frac{T_w - T_c}{\left(T_l - T_c\right) + \eta \frac{\gamma - 1}{2} M_\infty^2 T_l}$$

For simplicity, let $T_l = T_c = 500°$ R; $\eta = 0.88$ and $\gamma = 1.4$, then

$$\frac{T_w - T_c}{T_{aw} - T_c} = \frac{T_w - 500°}{88 M_\infty^2}$$

Values of this parameter are then calculated for a range of values for T_w and M_∞. The corresponding values for $\left(F/N_{St,o}\right)_{sw}$ are then read off the downstream or solid-wall cooling curve. Figure 15 shows the values of T_{sw} as a function of $\left(F/N_{St,o}\right)_{sw}$ for constant Mach number.

In determining the porous-wall values, the corresponding $F/N_{St,o}$ values are read off the porous-wall cooling curve. Figure 16 shows the Mach number variation with $\left(F/N_{St,o}\right)_{pw}$ for T_{pw} equal to 500° F, 900° F, and 1,400° F. In order to obtain curves, such as shown in figure 14, the Mach number and $\left(F/N_{St,o}\right)_{pw}$ values are read from figure 16

using the curve for the T_{pw} that is specified. Then from figure 15, the value of T_{sw} is read for the same numerical values of M and $F/N_{St,o}$. The ratio T_{sw}/T_{pw} is thereby determined as a function of Mach number for $\left(F/N_{St,o}\right)_{sw} = \left(F/N_{St,o}\right)_{pw}$ and Γ_{pw} constant.
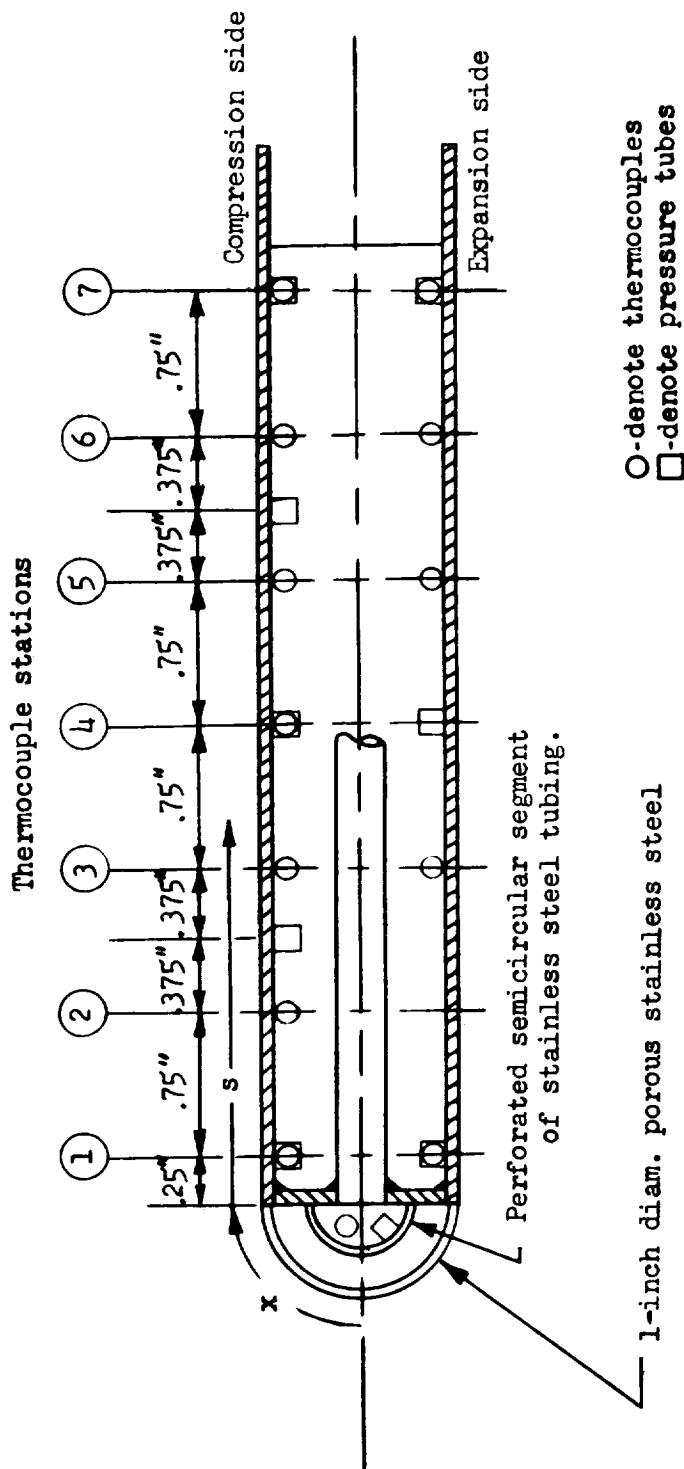
REFERENCES

1. Rashis, Bernard: Exploratory Investigation of Transpiration Cooling of a 40° Double Wedge Using Nitrogen and Helium as Coolants at Stagnation Temperatures of $1,295^\circ$ F to $2,910^\circ$ F. NACA RM L57F11, 1957.

2. Rashis, Bernard: Preliminary Indications of the Cooling Achieved by Ejecting Water Upstream From the Stagnation Point of Hemispherical, 80° Conical, and Flat-Faced Nose Shapes at a Stagnation Temperature of $4,000^\circ$ F. NACA RM L57I03, 1957.

3. English, Roland D., Spinak, Abraham, and Helton, Eldred H.: Physical Characteristics and Test Conditions of an Ethylene-Heated High-Temperature Jet. NACA TN 4182, 1958.

4. Goodwin, Glen, Creager, Marcus O., and Winkler, Ernest L.: Investigation of Local Heat-Transfer and Pressure Drag Characteristics of a Yawed Circular Cylinder at Supersonic Speeds. NACA RM A55H31, 1956.

5. Lewis Laboratory Computing Staff: Tables of Various Mach Number Functions for Specific-Heat Ratios From 1.28 to 1.38. NACA TN 3981, 1957.

6. Van Driest, E. R.: The Problem of Aerodynamic Heating. Aero. Eng. Rev., vol. 15, no. 10, Oct. 1956, pp. 26-41.

7. Keyes, F. G.: The Heat Conductivity, Viscosity, Specific Heat, and Prandtl Number for Thirteen Gases. Project SQUID, Tech. Rep. No. 37, M.I.T., Apr. 1, 1952.

Figure 1.- Model in jet.   L-58-3408.1

13

Thermocouple stations

Compression side

Expansion side

O-denote thermocouples
□-denote pressure tubes

Perforated semicircular segment
of stainless steel tubing.

1-inch diam. porous stainless steel

(a) Typical cross section.

Figure 2.- Detail drawing of model.

Bulkhead

Thermocouples

Pressure orifices

Porous stainless steel

Jet ℄

Backing plate

Perforated semicircular
segment of stainless
steel tubing

6.0"

8.5"

Helium supply lines
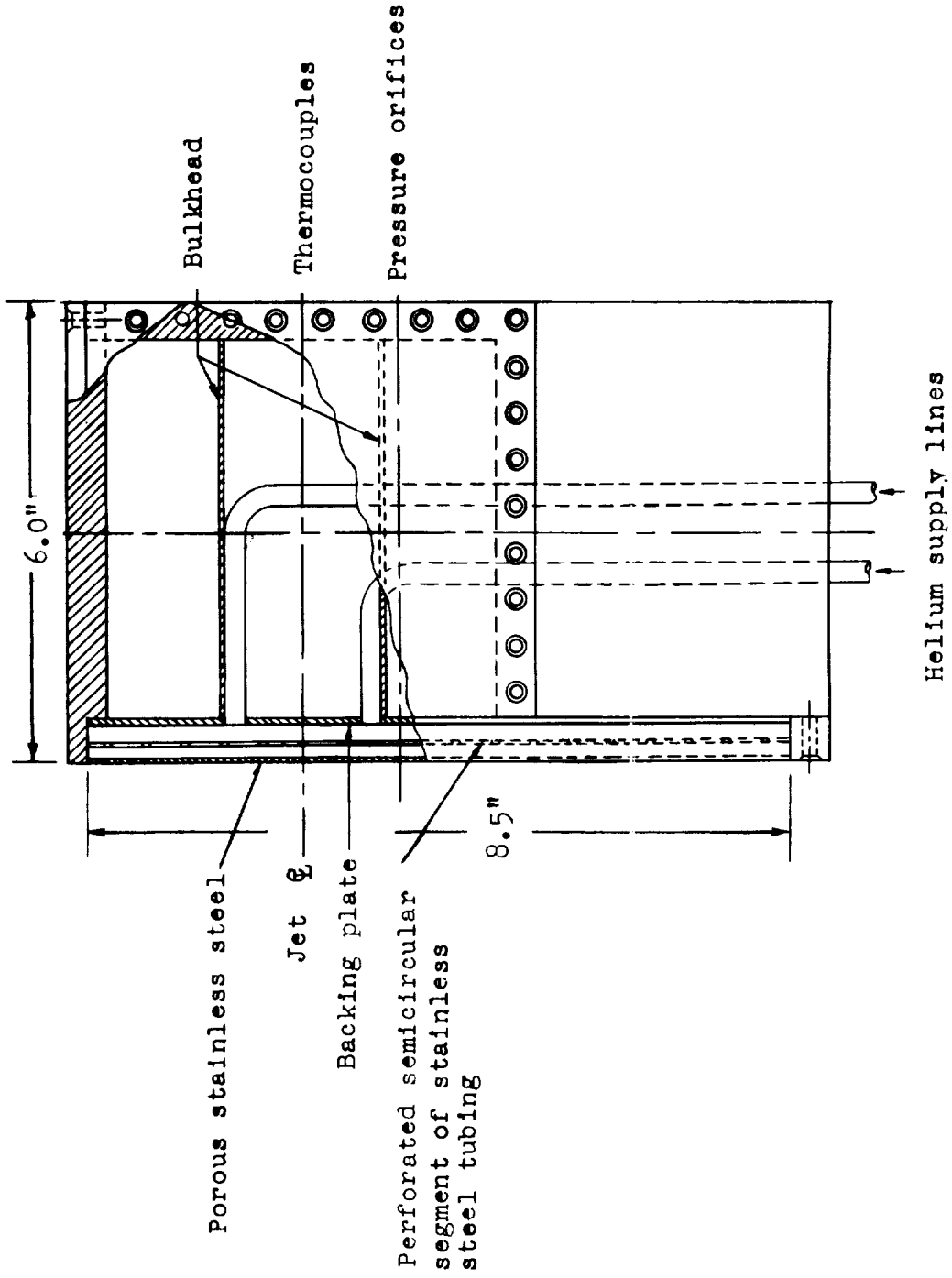
(b) Side view.

Figure 2.- Concluded.
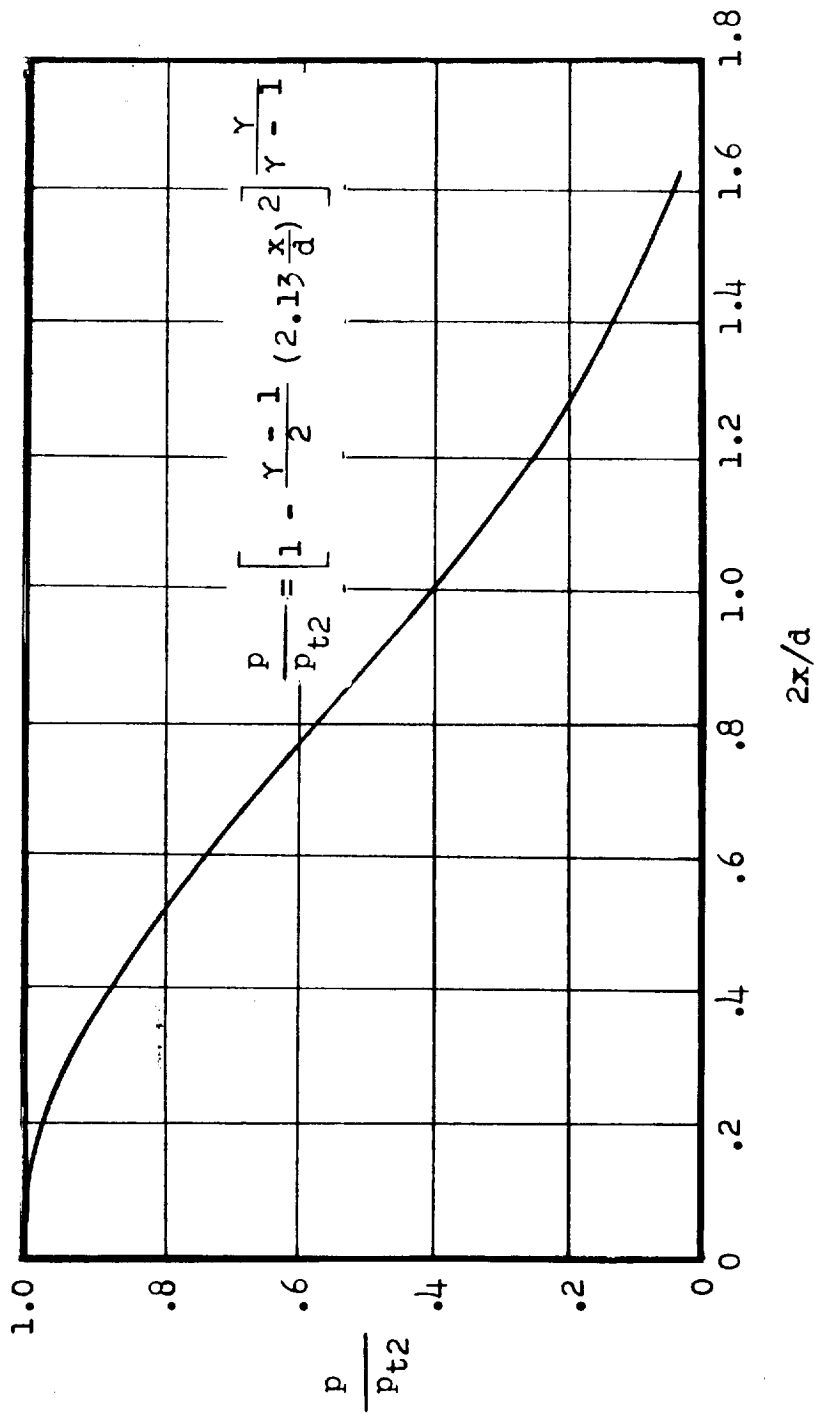
Figure 3.- The distribution of the ratios of surface pressure to a total pressure behind a normal shock over a leading edge of semicircular cross section. (Figure 9 from reference 4.)

$$\frac{p}{p_{t2}} = \left[1 - \frac{\gamma-1}{2}\left(2.13\frac{x}{d}\right)^2\right]^{\frac{\gamma}{\gamma-1}}$$
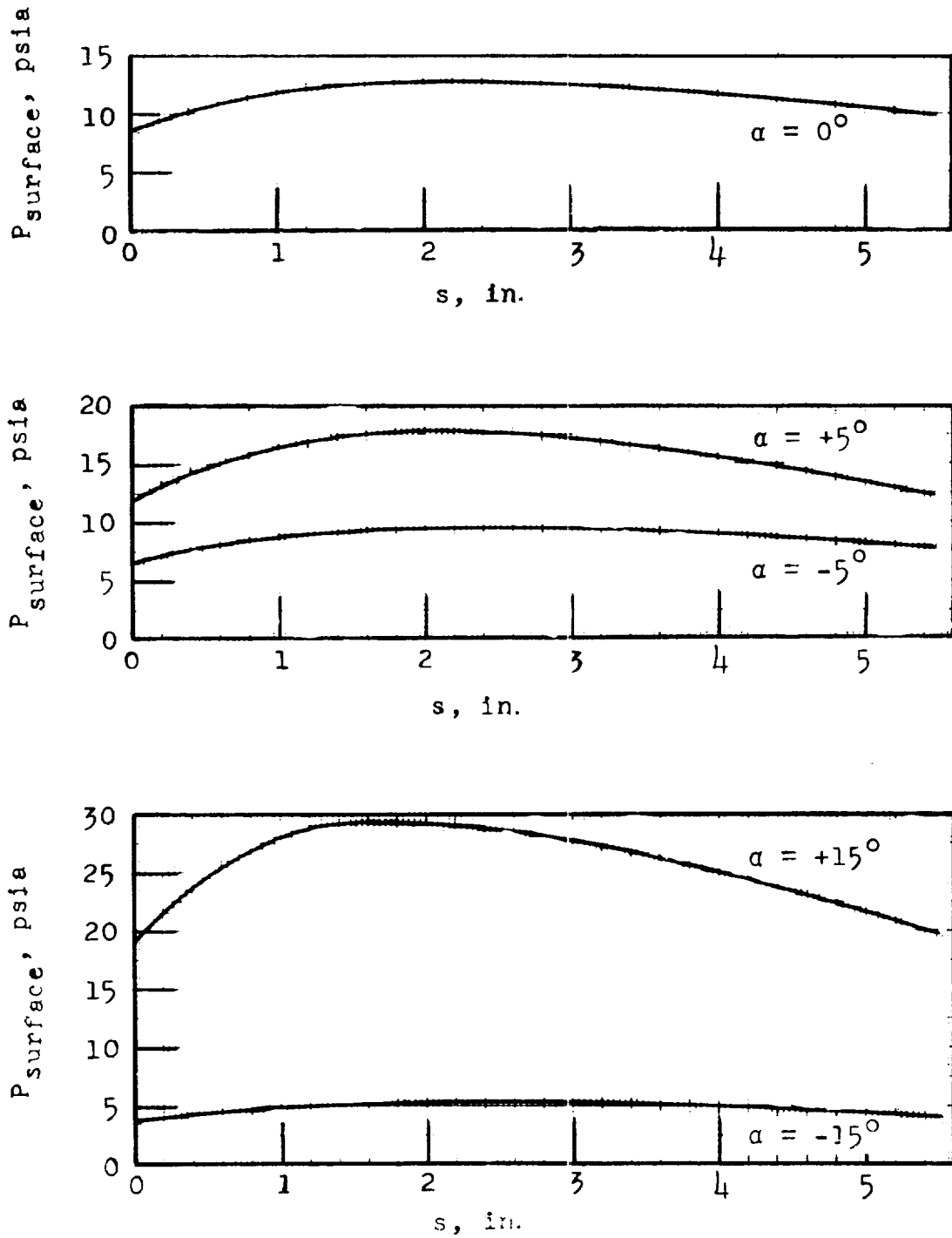
Figure 4.- The faired surface pressure distributions on the flat-plate
wing surfaces for $0°$, $5°$, and $15°$ angles of attack. $T_t = 1,000°$ F.
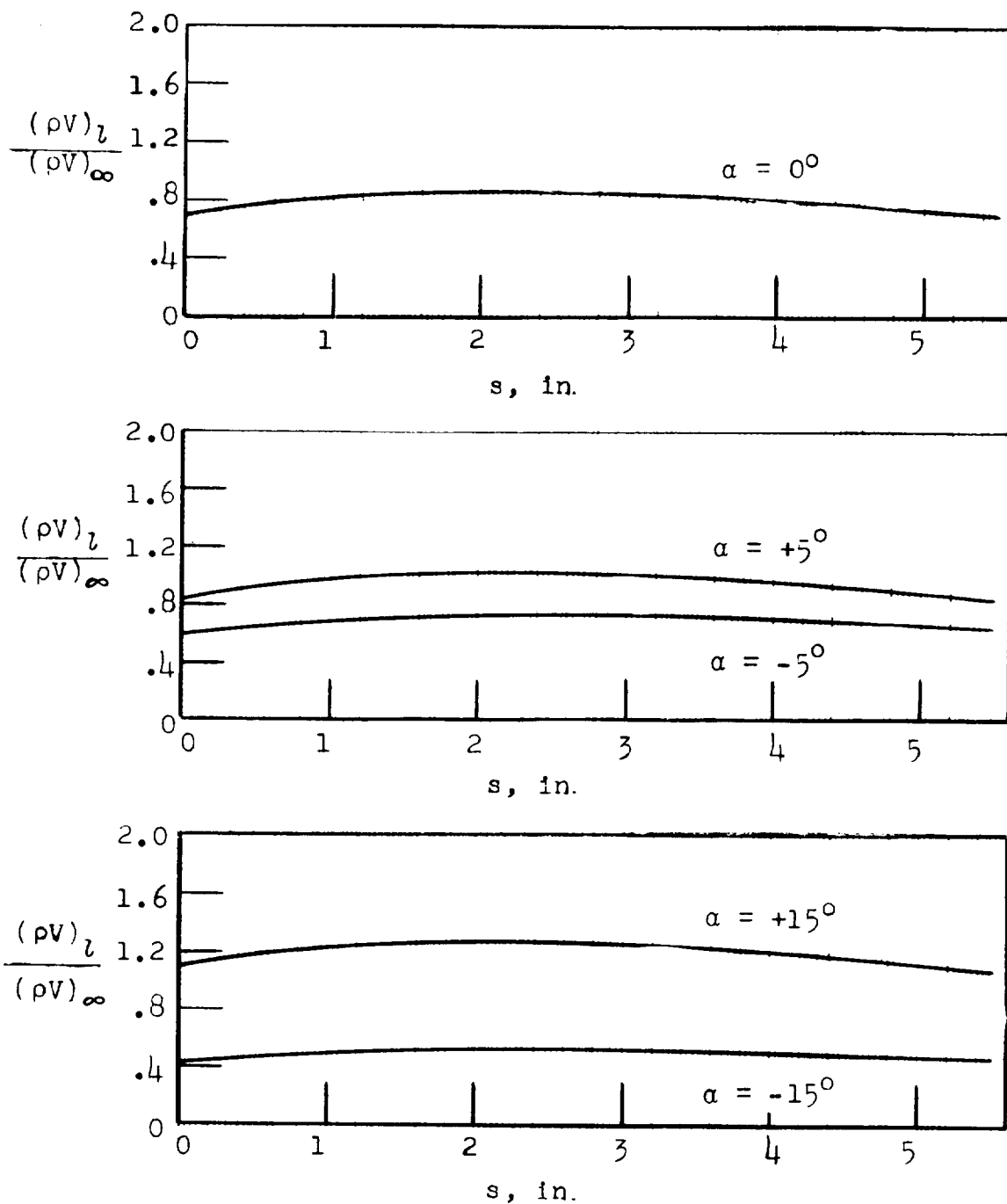
Figure 5.- The distributions of the ratios of local mass flow to free-stream mass flow over the flat-plate wing surfaces for 0°, 5°, and 15° angles of attack. $\gamma = 1.3$.
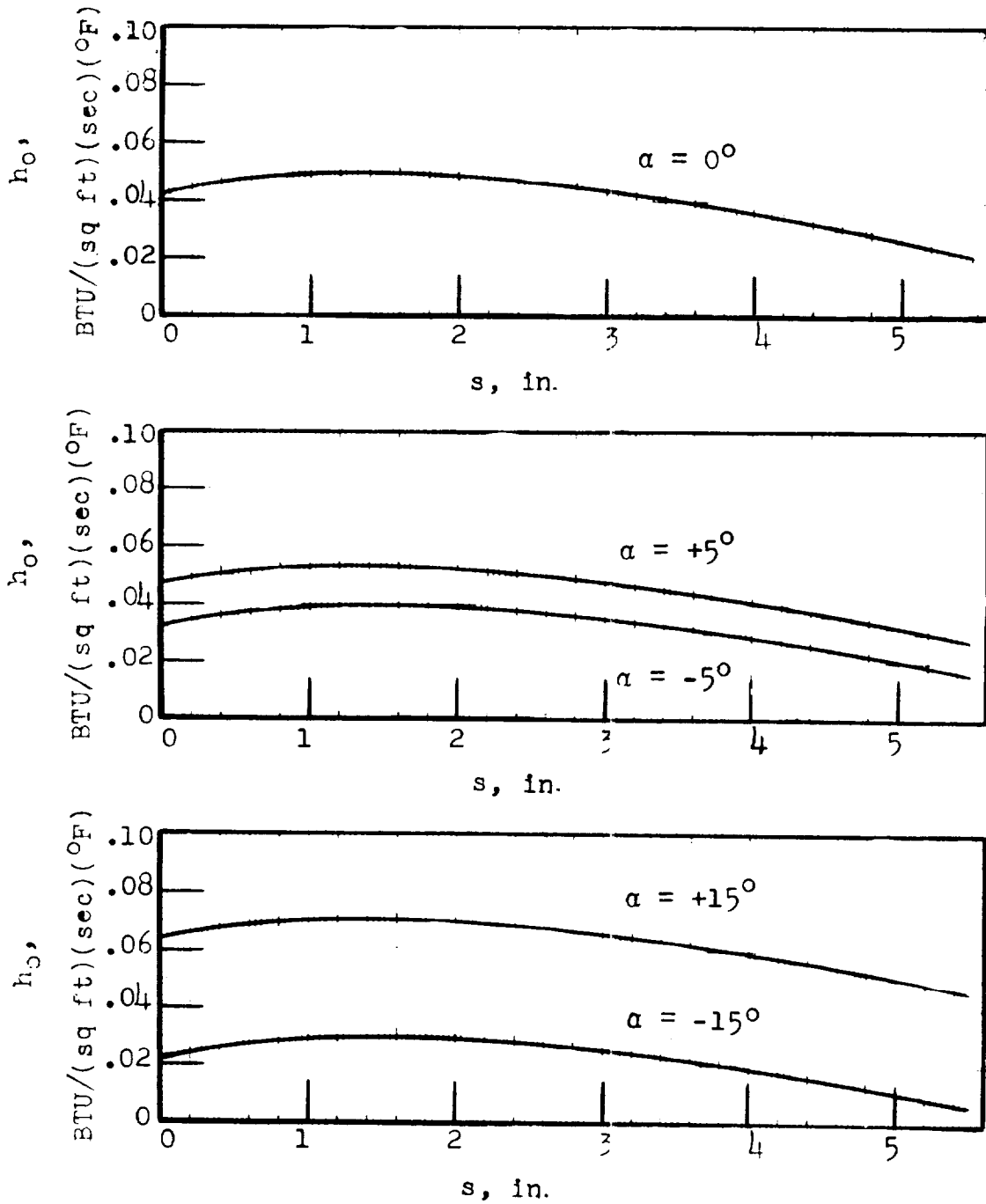
Figure 6.- The distribution of the zero-coolant-flow heat-transfer coefficients for angles of attack of $0°$, $5°$, and $15°$. $T_t \approx 1,000°$ F. $\gamma = 1.3$.
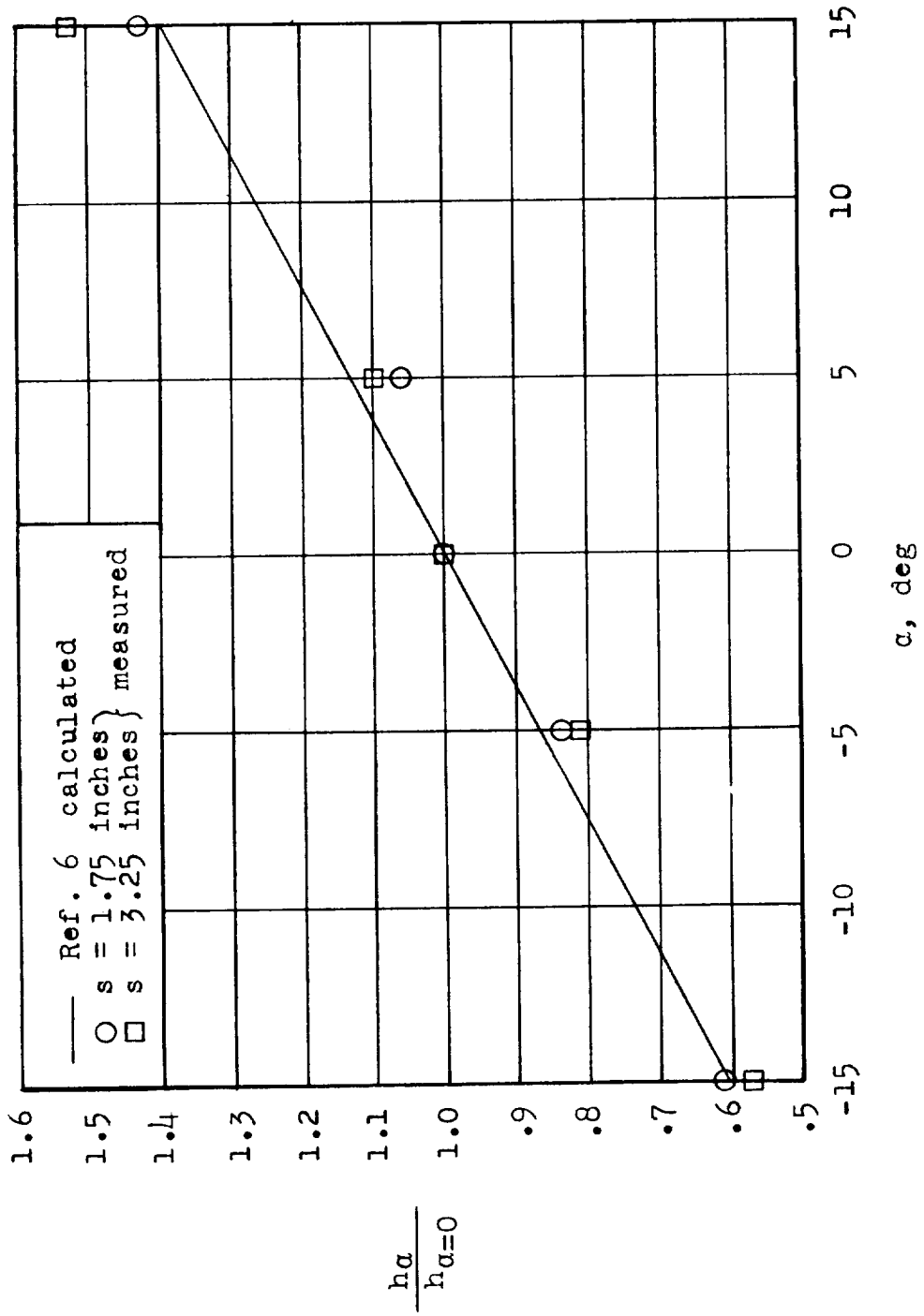
Figure 7.- Variation of the heat-transfer ratio as a function of angle of attack.
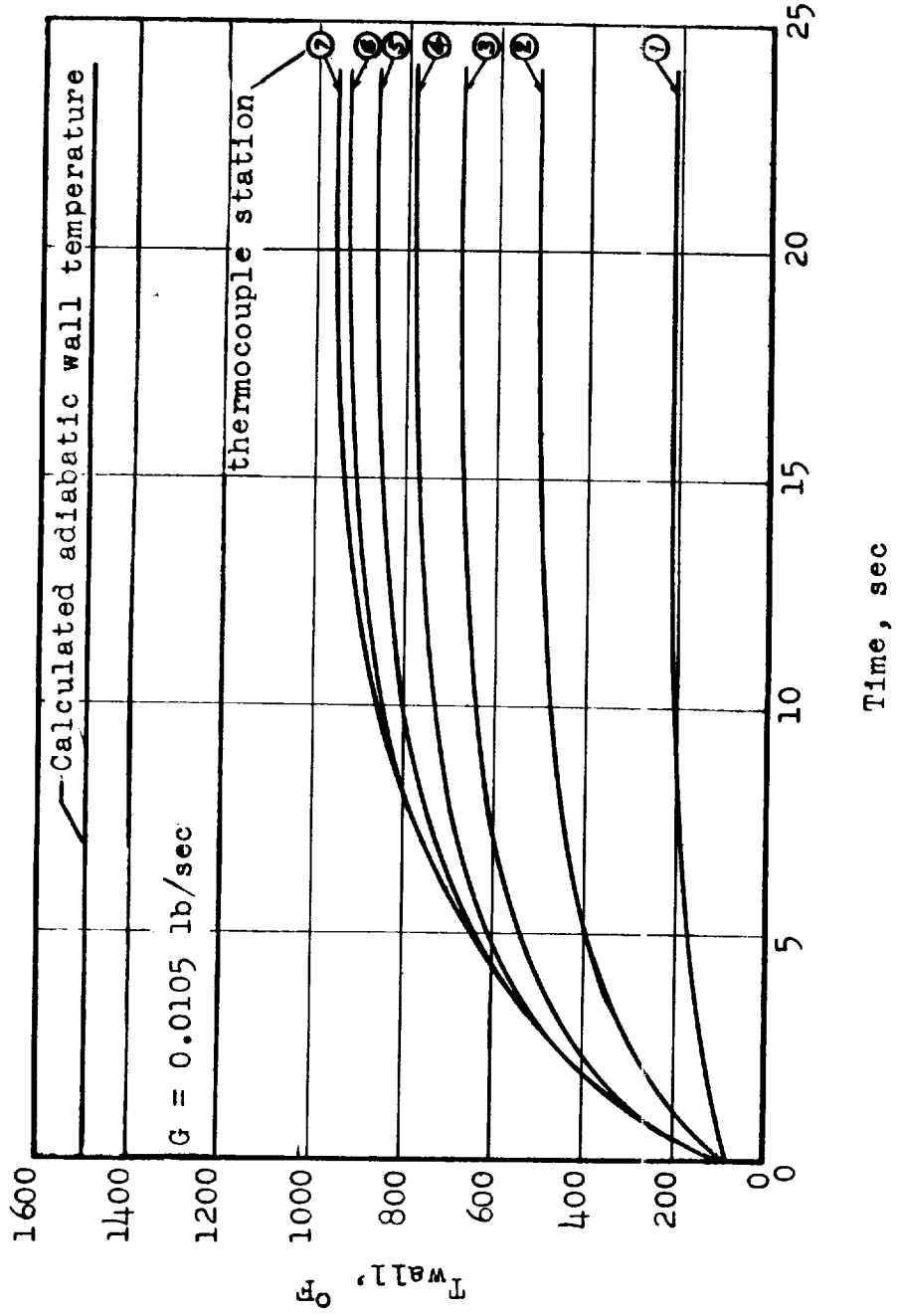
Figure 8.- A typical temperature time history for 0° angle of attack. $T_t = 1,588°$ F.
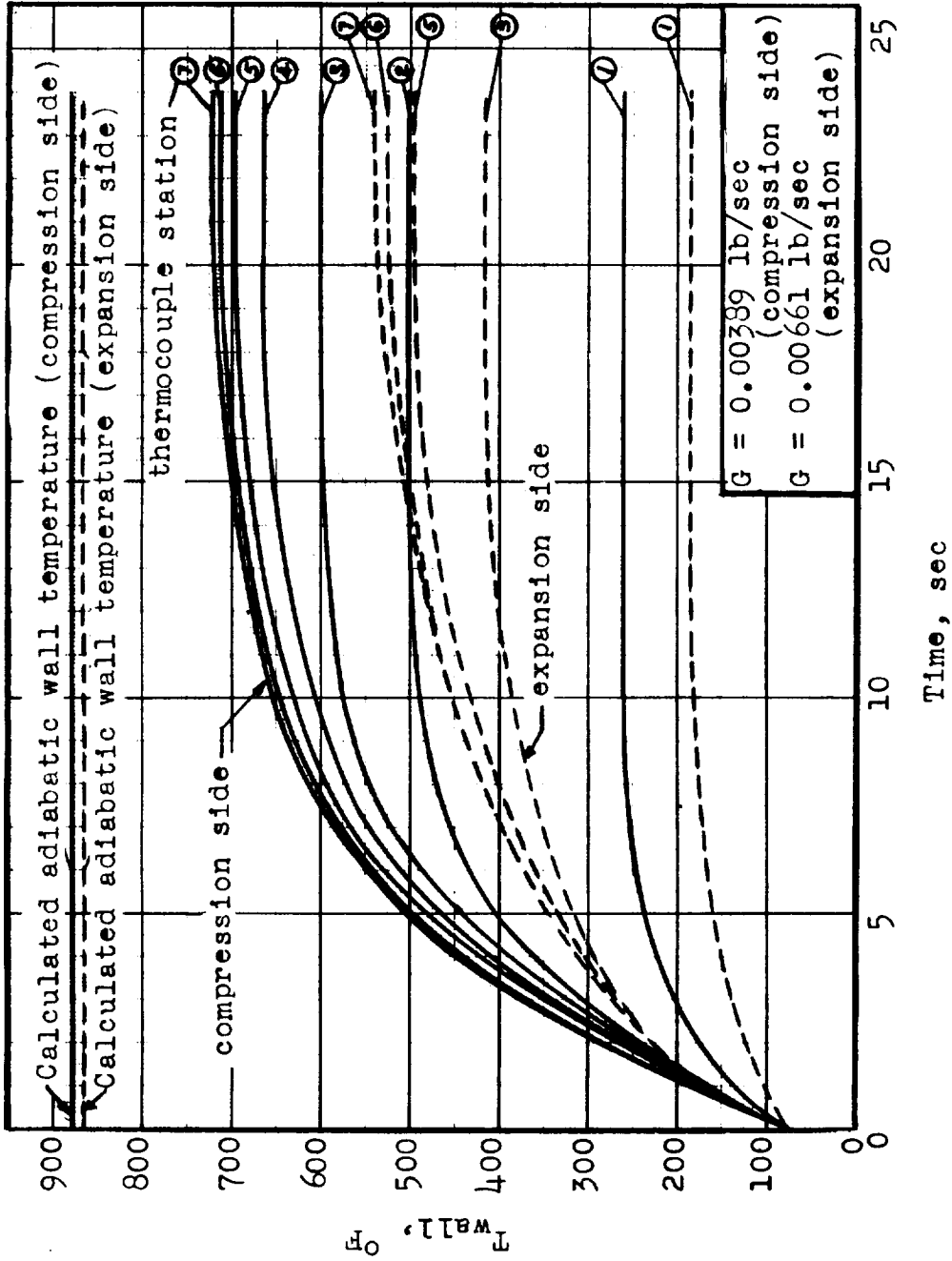
Figure 9.- A typical temperature time history for 5° angle of attack. $T_t = 935°$ F.
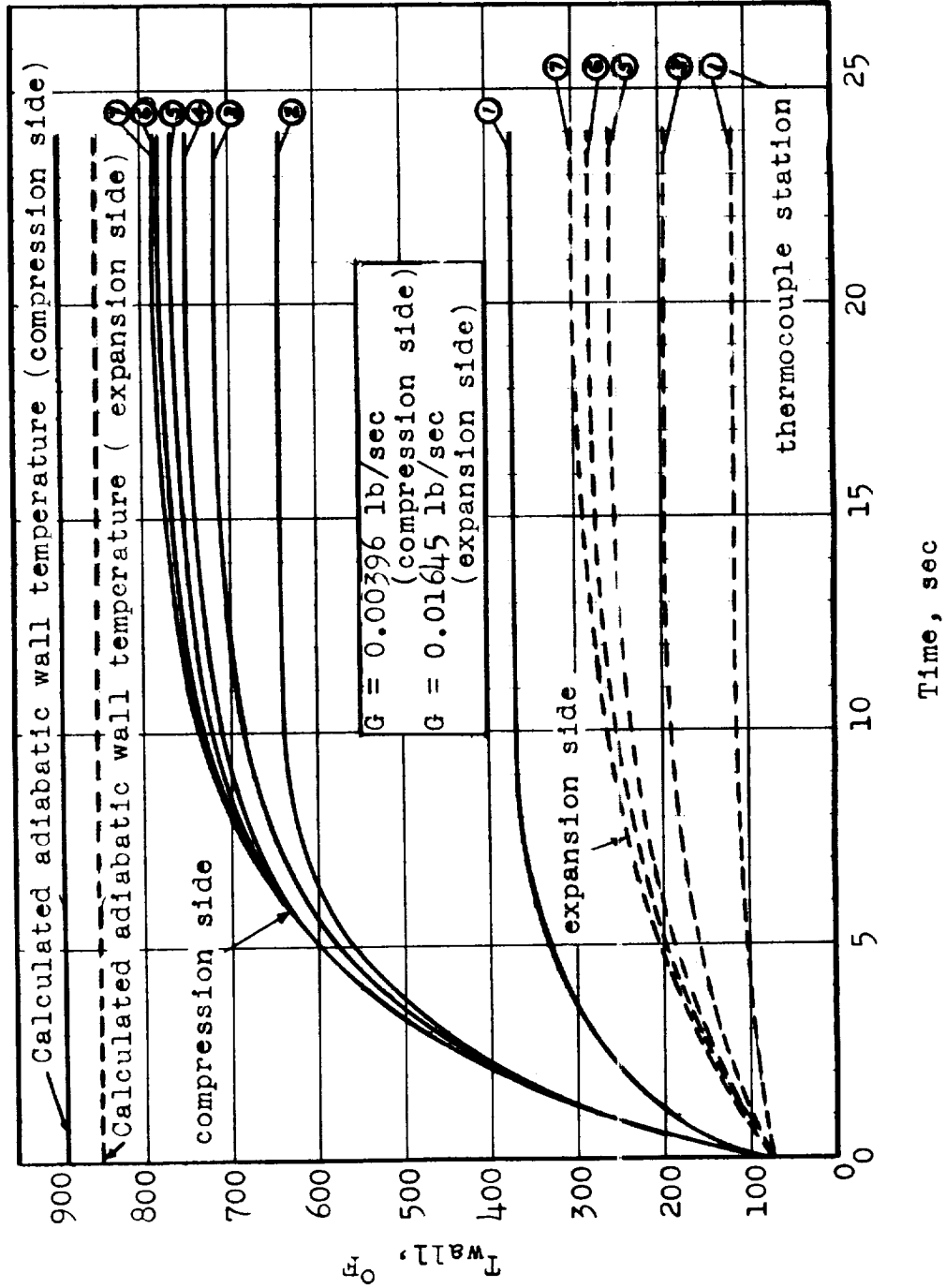
Figure 10.- A typical temperature time history for 15° angle of attack. $T_t = 935°$ F.
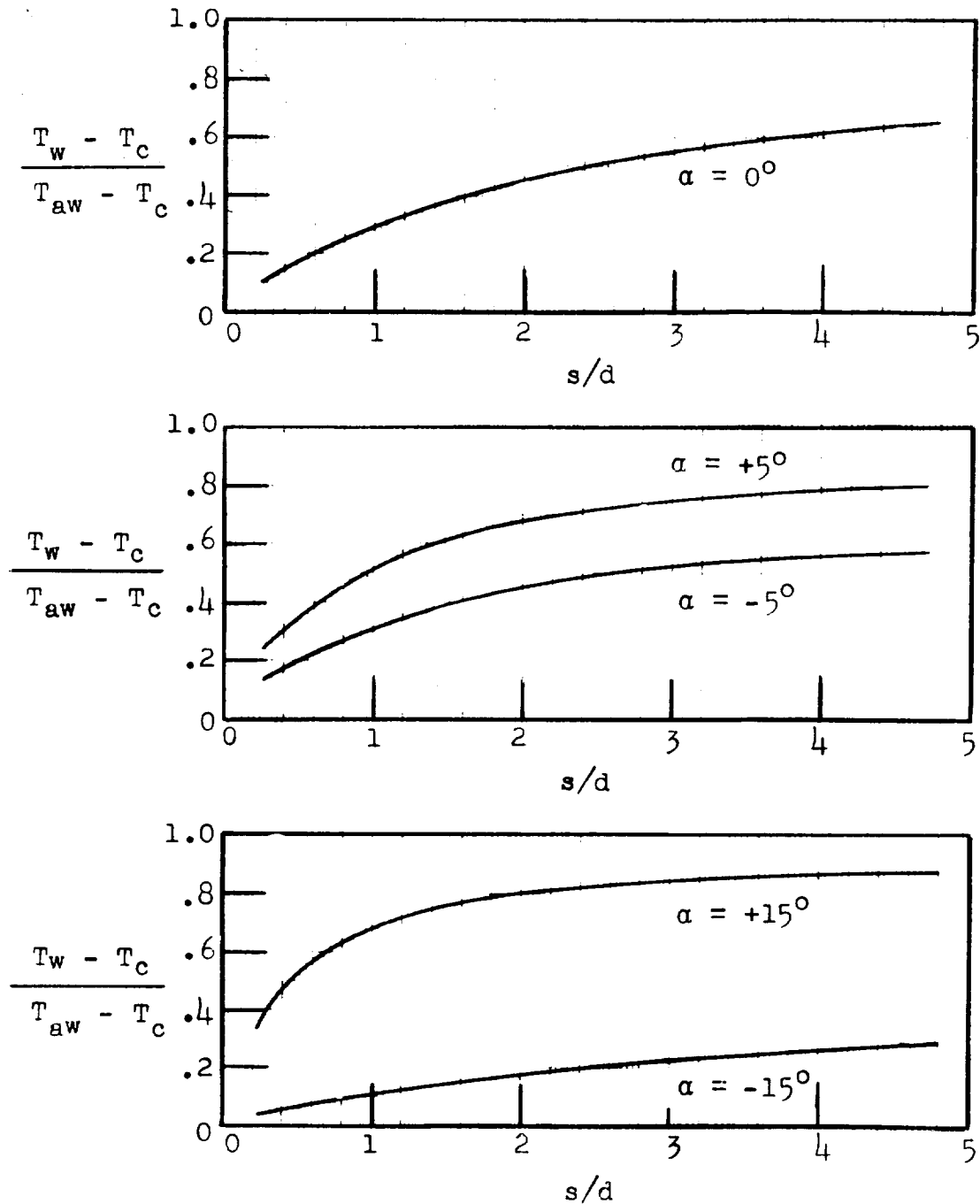
Figure 11.- The cooling efficiency parameter $(T_w - T_c)/(T_{aw} - T_c)$, plotted against s/d, the distance behind the porous leading-edge flat-plate juncture divided by the diameter of the leading edge.
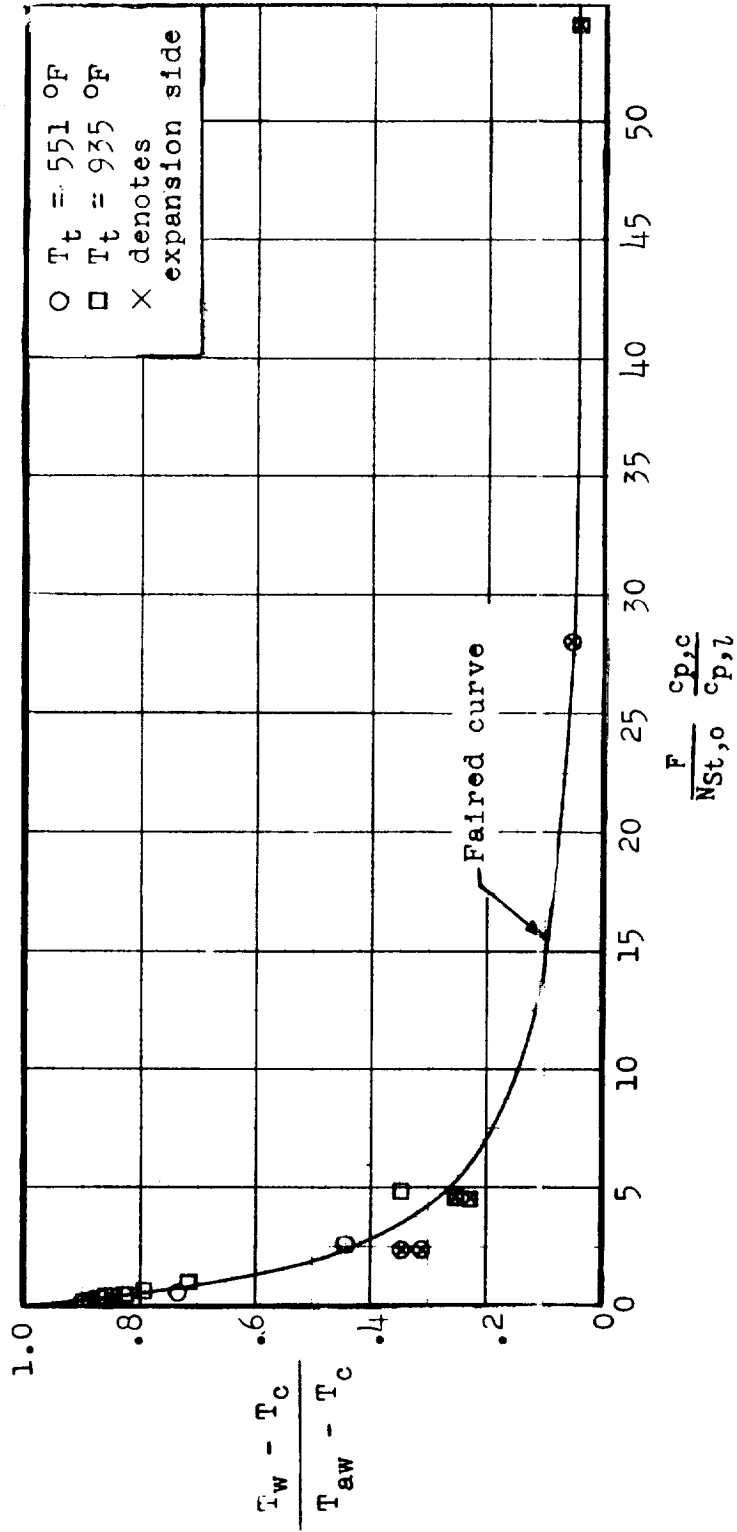
24
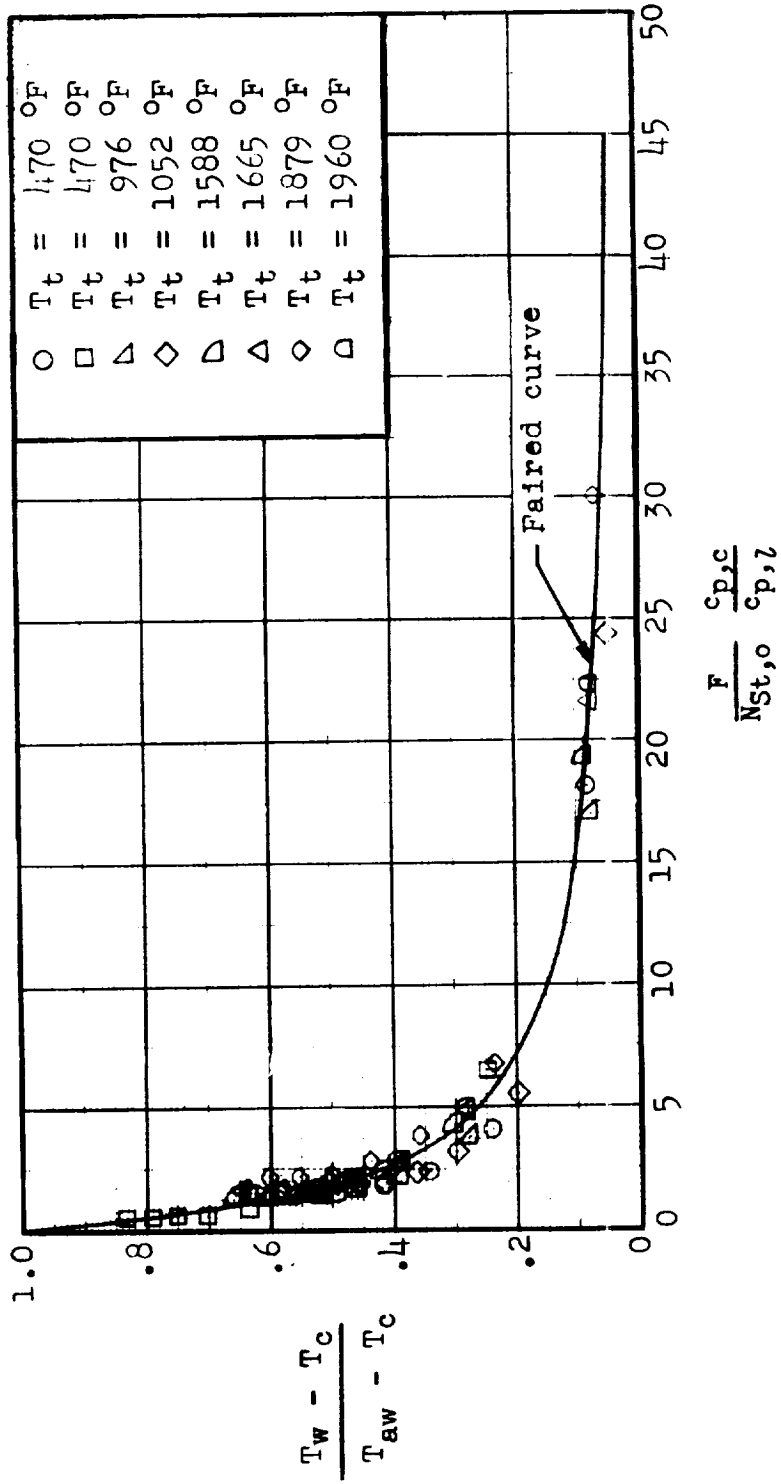
Figure 12.- The wall cooling parameter $(T_w - T_c)/(T_{aw} - T_c)$ plotted against the coolant flow-rate parameter $(F/N_{St,o})(c_{p,c}/c_{p,l})$.
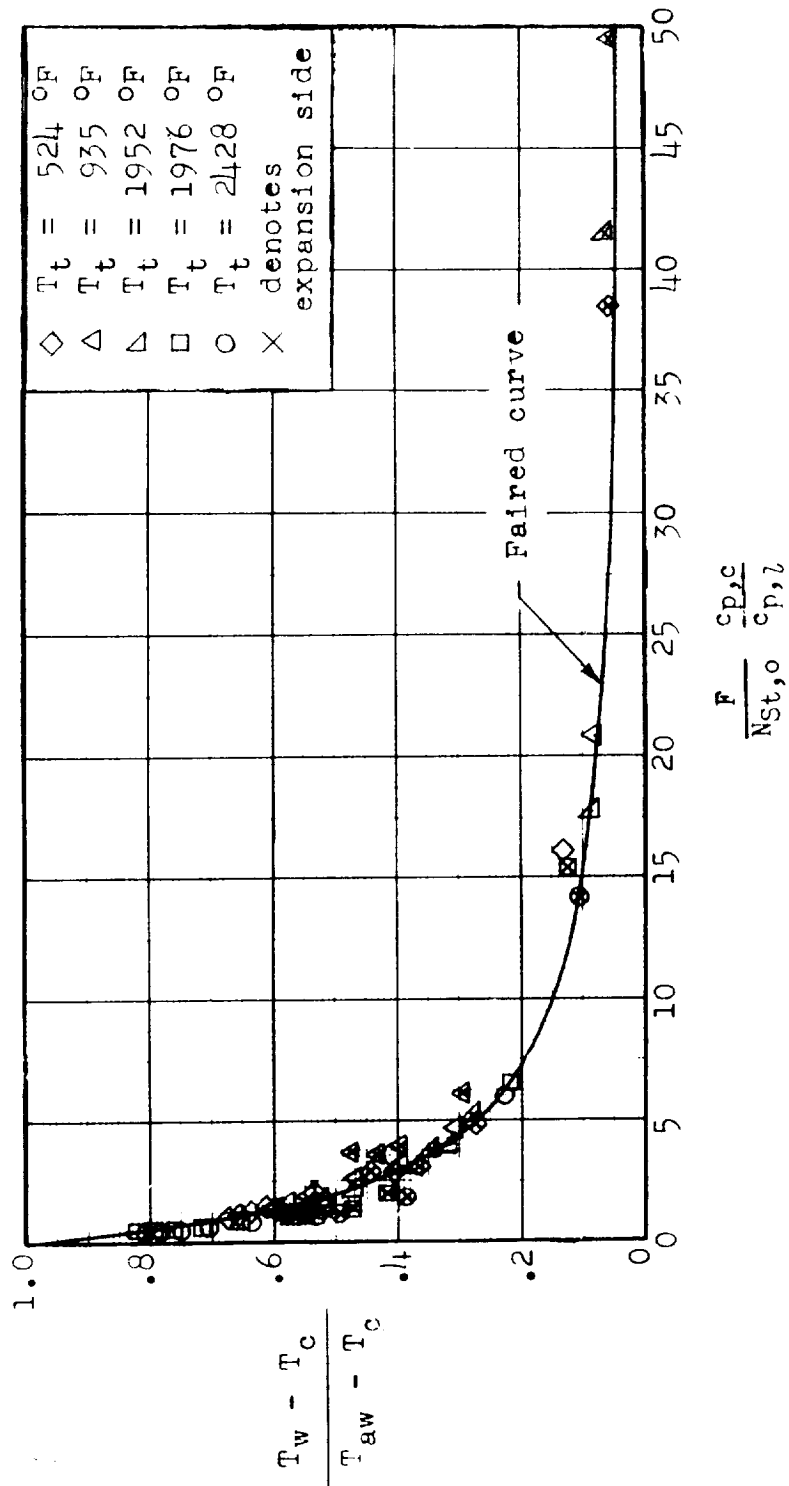
(a) $0°$ angle of attack.

(b) 5° angle of attack.

Figure 12.- Continued.
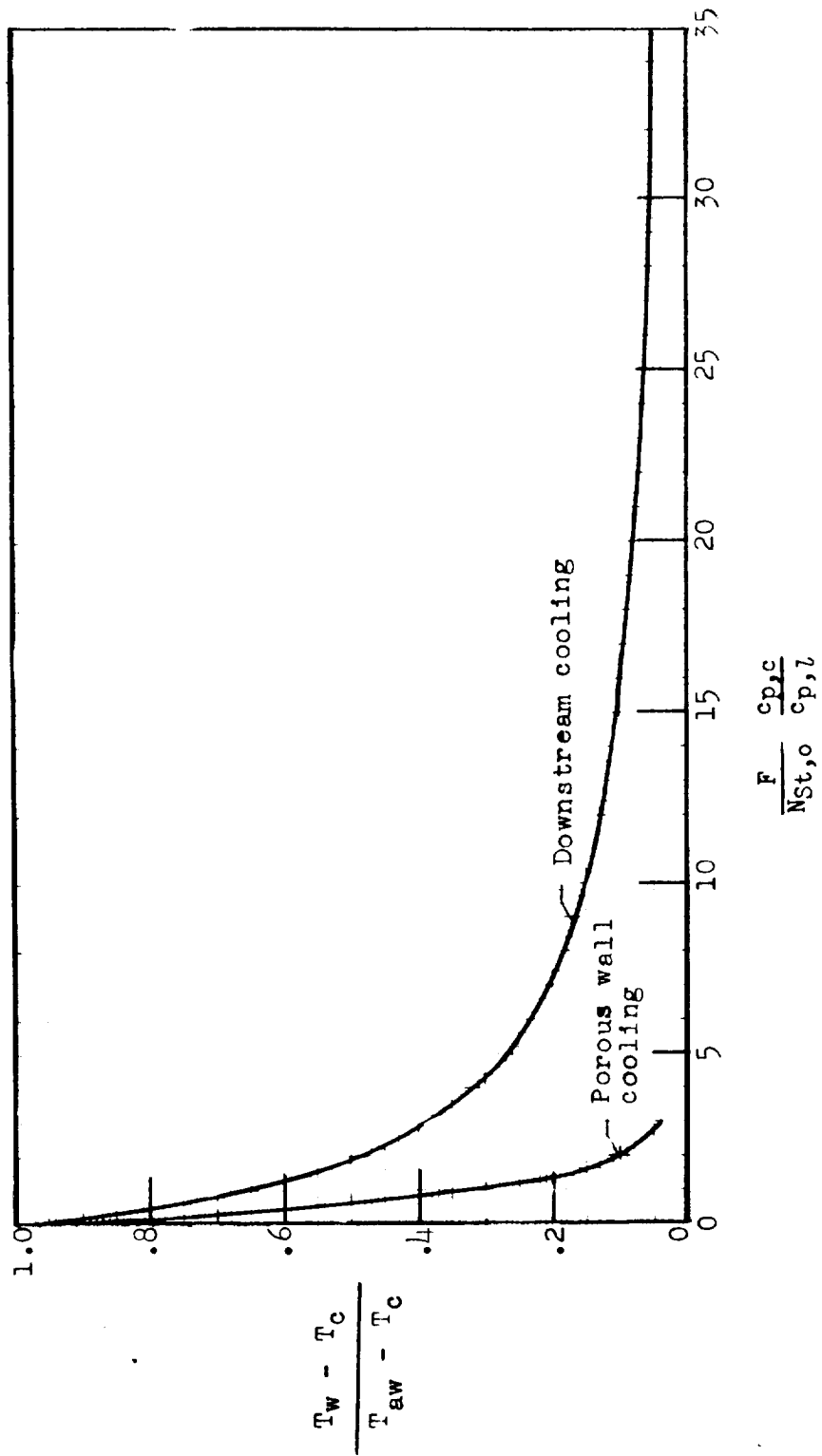
(c) 15° angle of attack.

Figure 12.- Concluded.

Figure 13.- Variation of wall cooling parameter with flow-rate correlation parameter for down-stream and porous wall cooling.
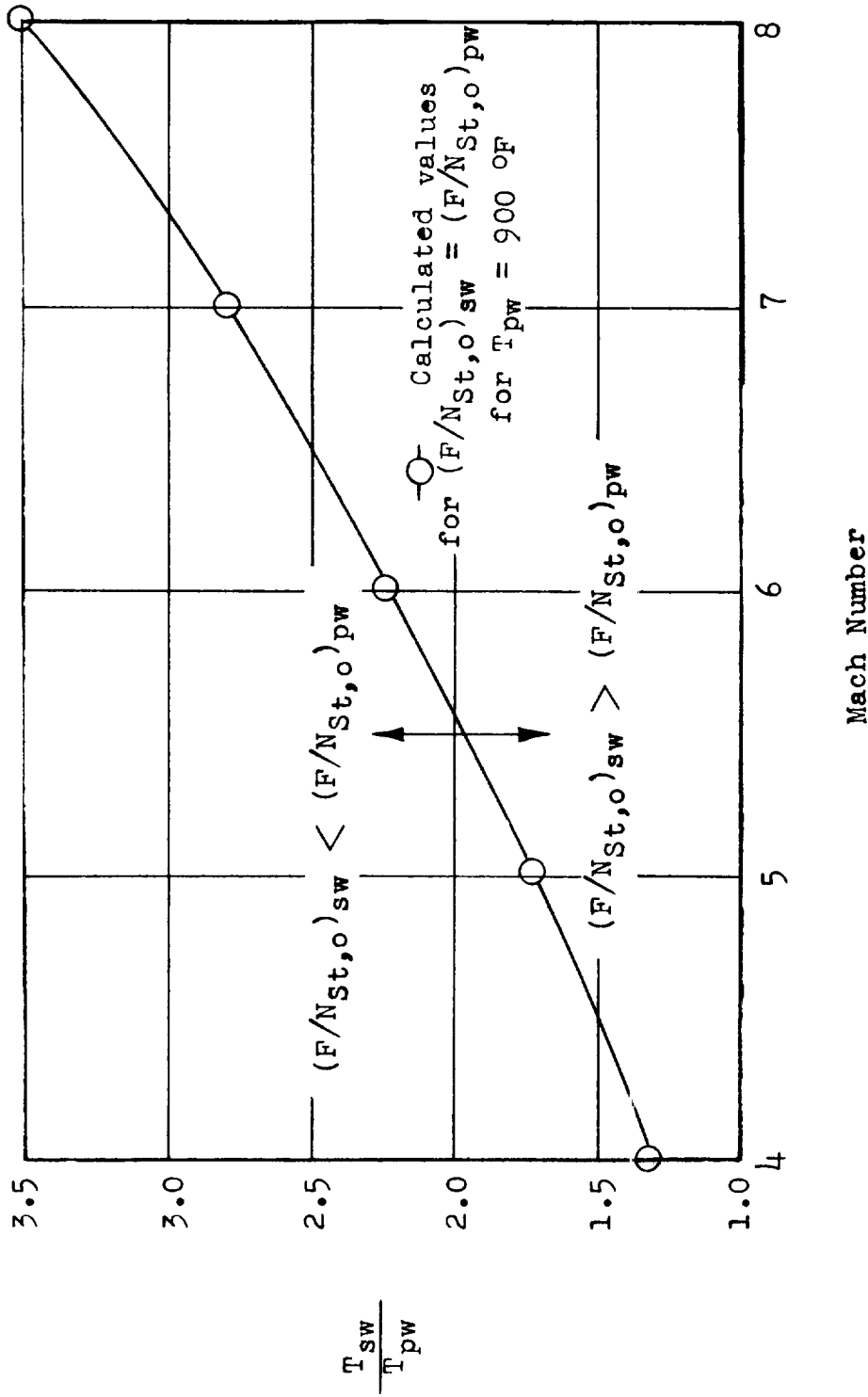
Figure 14.- Variation of T_{sw}/T_{pw} with Mach number for the case where $(F/N_{St,o})_{sw} = (F/N_{St,o})_{pw}$ when $T_{pw} = 900^\circ$ F.
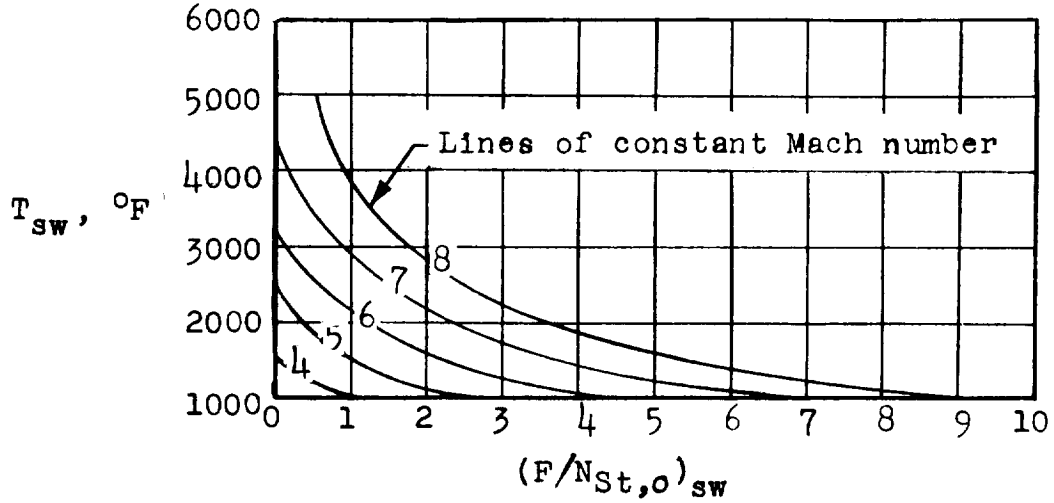
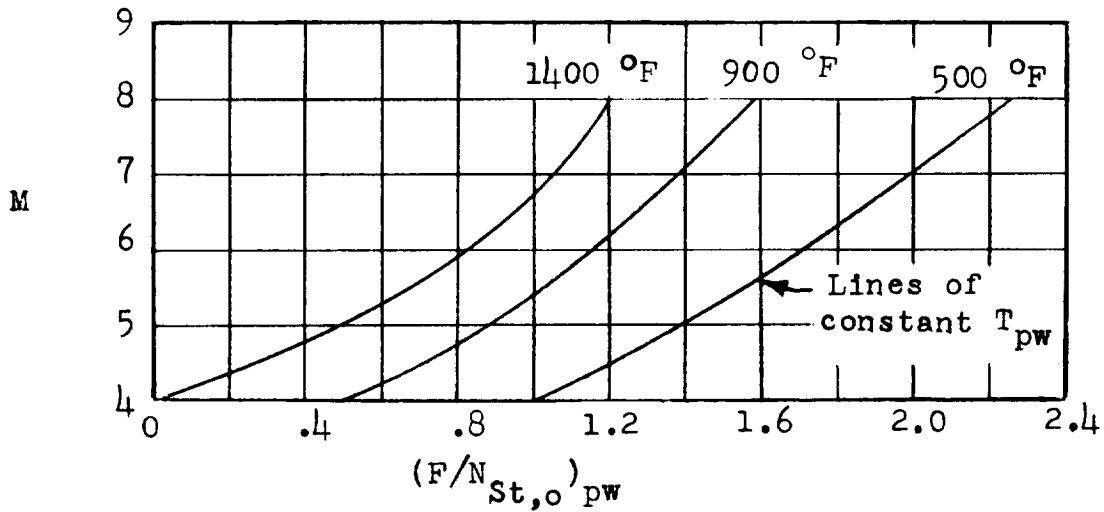Figure 15.- The variation of T_{sw} with $\left(F/N_{St,o}\right)_{sw}$ as a function of Mach number.

Figure 16.- Variation of Mach number with $\left(F/N_{St,o}\right)_{pw}$ as a function of T_{pw}.

NASA TM X-235
National Aeronautics and Space Administration.
AN EXPERIMENTAL INVESTIGATION AND COR-
RELATION OF THE HEAT REDUCTION TO NON-
POROUS SURFACES BEHIND A POROUS LEADING
EDGE THROUGH WHICH COOLANT IS EJECTED. March 1960.
William G. Witte and Bernard Rashis. March 1960.
29p. diagrs., photo.
(NASA TECHNICAL MEMORANDUM X-235)

(Title, Unclassified)

An experimental investigation of the downstream
cooling effectiveness of helium ejected through a
porous leading edge was conducted in a Mach num-
ber 2.0 ethylene-heated high-temperature air jet.
The configuration tested was a wing segment of con-
stant chord thickness and 0° sweep. Measurements
were made of the wing surface temperatures at
chordwise stations for several rates of helium flow
through the leading edge. The investigation was con-
ducted at stagnation temperatures up to 3,000° R, at
(over)

1. Heat Transfer, Aero-
   dynamic   (1.1.4.2)
2. Surface Conditions -
   Wing Sections
               (1.2.1.2.5)
I. Witte, William G.
II. Rashis, Bernard
III. NASA TM X-235

NASA

NASA TM X-235
National Aeronautics and Space Administration.
AN EXPERIMENTAL INVESTIGATION AND COR-
RELATION OF THE HEAT REDUCTION TO NON-
POROUS SURFACES BEHIND A POROUS LEADING
EDGE THROUGH WHICH COOLANT IS EJECTED. March 1960.
William G. Witte and Bernard Rashis. March 1960.
29p. diagrs., photo.
(NASA TECHNICAL MEMORANDUM X-235)

(Title, Unclassified)

An experimental investigation of the downstream
cooling effectiveness of helium ejected through a
porous leading edge was conducted in a Mach num-
ber 2.0 ethylene-heated high-temperature air jet.
The configuration tested was a wing segment of con-
stant chord thickness and 0° sweep. Measurements
were made of the wing surface temperatures at
chordwise stations for several rates of helium flow
through the leading edge. The investigation was con-
ducted at stagnation temperatures up to 3,000° R, at
(over)

1. Heat Transfer, Aero-
   dynamic   (1.1.4.2)
2. Surface Conditions -
   Wing Sections
               (1.2.1.2.5)
I. Witte, William G.
II. Rashis, Bernard
III. NASA TM X-235

NASA

NASA TM X-235
National Aeronautics and Space Administration.
AN EXPERIMENTAL INVESTIGATION AND COR-
RELATION OF THE HEAT REDUCTION TO NON-
POROUS SURFACES BEHIND A POROUS LEADING
EDGE THROUGH WHICH COOLANT IS EJECTED. March 1960.
William G. Witte and Bernard Rashis. March 1960.
29p. diagrs., photo.
(NASA TECHNICAL MEMORANDUM X-235)

(Title, Unclassified)

An experimental investigation of the downstream
cooling effectiveness of helium ejected through a
porous leading edge was conducted in a Mach num-
ber 2.0 ethylene-heated high-temperature air jet.
The configuration tested was a wing segment of con-
stant chord thickness and 0° sweep. Measurements
were made of the wing surface temperatures at
chordwise stations for several rates of helium flow
through the leading edge. The investigation was con-
ducted at stagnation temperatures up to 3,000° R, at
(over)

1. Heat Transfer, Aero-
   dynamic   (1.1.4.2)
2. Surface Conditions -
   Wing Sections
               (1.2.1.2.5)
I. Witte, William G.
II. Rashis, Bernard
III. NASA TM X-235

NASA

NASA TM X-235
National Aeronautics and Space Administration.
AN EXPERIMENTAL INVESTIGATION AND COR-
RELATION OF THE HEAT REDUCTION TO NON-
POROUS SURFACES BEHIND A POROUS LEADING
EDGE THROUGH WHICH COOLANT IS EJECTED. March 1960.
William G. Witte and Bernard Rashis. March 1960.
29p. diagrs., photo.
(NASA TECHNICAL MEMORANDUM X-235)

(Title, Unclassified)

An experimental investigation of the downstream
cooling effectiveness of helium ejected through a
porous leading edge was conducted in a Mach num-
ber 2.0 ethylene-heated high-temperature air jet.
The configuration tested was a wing segment of con-
stant chord thickness and 0° sweep. Measurements
were made of the wing surface temperatures at
chordwise stations for several rates of helium flow
through the leading edge. The investigation was con-
ducted at stagnation temperatures up to 3,000° R, at
(over)

1. Heat Transfer, Aero-
   dynamic   (1.1.4.2)
2. Surface Conditions -
   Wing Sections
               (1.2.1.2.5)
I. Witte, William G.
II. Rashis, Bernard
III. NASA TM X-235

NASA

NASA TM X-235

Reynolds numbers per foot ranging from 0.3×10^7 to 1.2×10^7, and at angles of attack of $0°$, $5°$, and $15°$.

NASA

NASA TM X-235

Reynolds numbers per foot ranging from 0.3×10^7 to 1.2×10^7, and at angles of attack of $0°$, $5°$, and $15°$.

NASA

NASA TM X-235

Reynolds numbers per foot ranging from 0.3×10^7 to 1.2×10^7, and at angles of attack of $0°$, $5°$, and $15°$.

NASA

NASA TM X-235

Reynolds numbers per foot ranging from 0.3×10^7 to 1.2×10^7, and at angles of attack of $0°$, $5°$, and $15°$.

NASA